Materials Horizons

COMMUNICATION

Published on 06 February 2026
Licence and permissions

Check for updates

Cite this: *Mater. Horiz.*, 2026, **13**, 3880

Received 17th November 2025, Accepted 20th January 2026

DOI: 10.1039/d5mh02182k

rsc.li/materials-horizons

High-dimensional multiplexed metamaterial for cross-media all-sound communication

Kai Wu, †[a] Jing-Jing Liu, †*[a] Hao-Xiang Li, [b] Xue-Feng Zhu, [c] Bin Liang, *[a] Jian-Chun Cheng *[a] and Johan Christensen *[d]

Direct transmission of information-carrying sound waves across different states of matter holds significant implications for diverse disciplines. However, existing natural and artificial materials can modulate only one or a few dimensions of cross-media sound waves, imposing inherent bottlenecks on transmission rate and information density. Here, we propose a high-dimensional multiplexed (HDM) metamaterial capable of modulating all dimensions of cross-water–air sound waves including amplitude, phase, frequency, and orbital angular momentum in a passive, compact and efficient way. Thanks to this high-dimensional characteristic, the monolayered HDM metamaterial with subwavelength thickness enables simultaneously relaying and demodulating the spatial-spectral multiplexed signals from one medium to another, which significantly enhances channel capacity and spectral efficiency. We experimentally demonstrate an example of cross-water–air all-sound communication with the HDM metamaterial serving as a passive meta-repeater by transmitting a complex image encoded in both spatial and spectral domains through the metamaterial-based water–air communication link, showcasing real-time, high-speed, and postprocessing-free communication with a bit error rate near 1/10 of the forward error correction limit and strong robustness against background noise and fluctuating surface. This HDM metamaterial-based technique opens a new paradigm for sound wave control in complicated cross-media systems, with far-reaching implications in the Internet of Everything and beyond.

[a] *Collaborative Innovation Center of Advanced Microstructures and Key Laboratory of Modern Acoustics, MOE, Institute of Acoustics, Department of Physics, Nanjing University, Nanjing 210093, China. E-mail: liujingjing@nju.edu.cn, liangbin@nju.edu.cn, jccheng@nju.edu.cn*

[b] *College of Information Science and Technology & College of Artificial Intelligence Nanjing Forestry University, Nanjing 210037, China*

[c] *School of Physics and Innovation Institute, Huazhong University of Science and Technology, Wuhan 430074, China*

[d] *IMDEA Materials Institute, Calle Eric Kandel, 2, Getafe, Madrid 28906, Spain. E-mail: johan.christensen@imdea.org*

† Kai Wu and Jing-Jing Liu contributed equally to this work.

New concepts

Matter serves as the indispensable condition for acoustic wave propagation; however, the significant disparities in acoustic properties among different material phases (*viz.*, gas, liquid, and solid) have long hindered the cross-media transmission of acoustic energy and information. Although recently emerging acoustic metamaterials have been proven capable of breaking the sound transmission barrier of the water–air interface just like opening an "acoustic window", they can modulate only one or few dimensions of cross-media sound waves, limiting their application in diverse important scenarios. This study reports a HDM acoustic metamaterial that enables modulating all dimensions of sound waves traversing water–air media, including amplitude, phase, frequency and OAM. Thanks to this high-dimensional characteristic, our approach significantly boosts channel capacity and spectral efficiency in cross-media system by introducing OAM-based spatial multiplexing and frequency-based spectral multiplexing. Experimentally, we demonstrate real-time and high-speed transmission of a complex image from one underwater node to multiple airborne nodes *via* a HDM metamaterial-based passive meta-repeater that supports four independent channels. This work establishes a new paradigm for extending the multi-dimensional sound manipulation to complex cross-media systems, paving the way for future applications in areas such as transcranial ultrasound imaging and beyond.

1. Introduction

Matter is essential for the propagation of sound waves, yet the significant differences in acoustic properties across different states of matter (gas, liquid, solid) present considerable challenges for cross-media transmission of sound.[1–4] For instance, the large differences in density and sound speed between water and air prevent synchronized swimming athletes from hearing music played in the air when diving underwater, necessitating the use of another underwater speaker to synchronize dance movements. Achieving direct transmission of sound information across different states of matter holds critical significance for various fields.[5–7] One typical and highly relevant example is establishing a robust and high-speed all-sound communication link between water and air, which is appealing for modern communication technology and plays a key role in a wide range of applications spanning from joint air–sea rescue and offshore petroleum exploration to cross-media remote sensing. This calls for the effective control of as many dimensions of cross-media sound waves as possible to ensure important performances in terms of coding degree of freedom (DoF), and communication speed, among others, which, however, is beyond attainable with the existing materials. To be specific, natural acoustic materials, constrained by their microscopic internal molecular structure and macroscopic physical properties, can only enhance the sound transmission efficiency between water and air to a certain extent based on methods such as quarter-wavelength resonance matching,[8,9] whereas the resonance-induced phase and frequency-locking limit inherently their ability to modulate other dimensions of sound waves beyond amplitude. Recently, acoustic metamaterials engineered with special structural designs and exhibiting exceptional properties not found in nature[10–18] have been proven feasible for breaking the sound transmission barrier of the water–air interface just like opening an ''acoustic window'' with the transmitted sound fields being molded at will.[19–32] However, most of them are designed for only one single frequency or ignore the insight into orbital angular momentum modulation (OAM,[33–41] an emerging coding DoF for spatial multiplexing). Hence, both traditional natural materials and advanced acoustic metamaterials are incapable of simultaneously modulating all dimensions of cross-media sound waves, *i.e.*, amplitude, phase, frequency, and OAM, which restricts the effective interaction range, energy transmission efficiency, and information transfer rate of sound waves across different media.

Considering the aforementioned challenges, the existing methods for cross-media communications usually require active repeaters such as floating buoys, ships or other surface vehicles to receive underwater information carried by sound waves and relay it to airborne radio signals.[42–44] In addition to the time-consuming carrier conversion and high cost, the transmission of airborne signals poses potential risks caused by electromagnetic interference and wiretapping from third parties. Despite some emerging techniques providing an alternative of cross-media communications without relay devices, such as laser-induced sound systems and line-of-sight optical links, their applications in real-world systems are often limited by the need for precise alignment and tranquil sea surface.[45] Consequently, there is a compelling interest in broadening the controllable dimensions of cross-media sound waves and establishing a new cross-media communication paradigm capitalizing on acoustic waves as the unique carrier, which nevertheless remains an immediate unresolved undertaking.

In this article, we develop a novel high-dimensional multiplexed (HDM) metamaterial for modulating all dimensions of sound waves traversing water–air media and realize, for the first time, cross-media all-sound communication in a real-time, high-speed and no-carrier-conversion paradigm. The proposed HDM metamaterial, acting as a sound communication bridge between water and air, enables efficiently and directly converting high-dimensional multiplexed waterborne sound signals into demultiplexed airborne sound signals through precise modulation on all-dimensional information of cross-media waves. Specifically, it can independently provide each operating frequency component with effective energy enhancement by up to 156 times and arbitrary phase delay within the 0 to 2π range, thereby achieving simultaneous amplitude, phase and frequency modulation. In parallel, the assembly of such a HDM metamaterial also allows for engineering the topological charge of the incident vortex beam, *viz.*, OAM modulation. The underlying working mechanism can be elucidated as follows: the multilayered impedance design of the HDM metamaterial in the propagation direction effectively overcomes the inherent resonance phase locking of single-layered structures, while the spatial hybridization of different resonant elements perpendicular to the propagation direction increases the density of resonance states and thereby extends the working frequency range. Thanks to this high-DoF characteristic, our approach significantly boosts channel capacity and spectral efficiency by introducing additional coding DoFs, including OAM-based spatial multiplexing and spectral multiplexing. The experimental realization for real-time transmission of a complicated image from one underwater node to four airborne nodes is demonstrated through an HDM metamaterial-based meta-repeater with four independent channels (two OAM channels × two spectral channels), showcasing the accurate decoding of multiplexed signals, an extremely low bit error rate (BER) [much lower than 1/10 of the forward error correction (FEC) limit[46]], and high robustness against background noise and water surface fluctuation. Besides, given the fact that such a mechanism can operate in the absence of radio signals, its security and reliability become unaffected by potential risks induced by factors such as electromagnetic interference and eavesdropping, with pivotal significance in practical applications.

2. Results and discussion

2.1. The mechanism of HDM metamaterial for all-dimensional modulation on cross-media sound waves

Fig. 1 schematically illustrates how our proposed HDM metamaterial works as an acoustic bridge linking water and air for all-dimensional sound manipulation and cross-media all-sound communication. Given the inherently fewer controllable dimensions of sound waves compared to electromagnetic waves, fully exploiting all available dimensions of sound waves is essential for various acoustic applications, such as sound field manipulation, high-capacity holography, and high-speed sound communication. Normally, when sound waves illuminate the water–air interface, they mostly reflect back due to the extreme acoustic impedance mismatch between water and air, just like light impinging on a mirror. By decorating the water–air interface with impedance-matching materials, the acoustic barrier of cross-media transmission can be broken through. Beyond such energy enhancement, the simultaneous modulation/demodulation on the other relevant dimensions of sound waves traversing different media is also highly desired yet

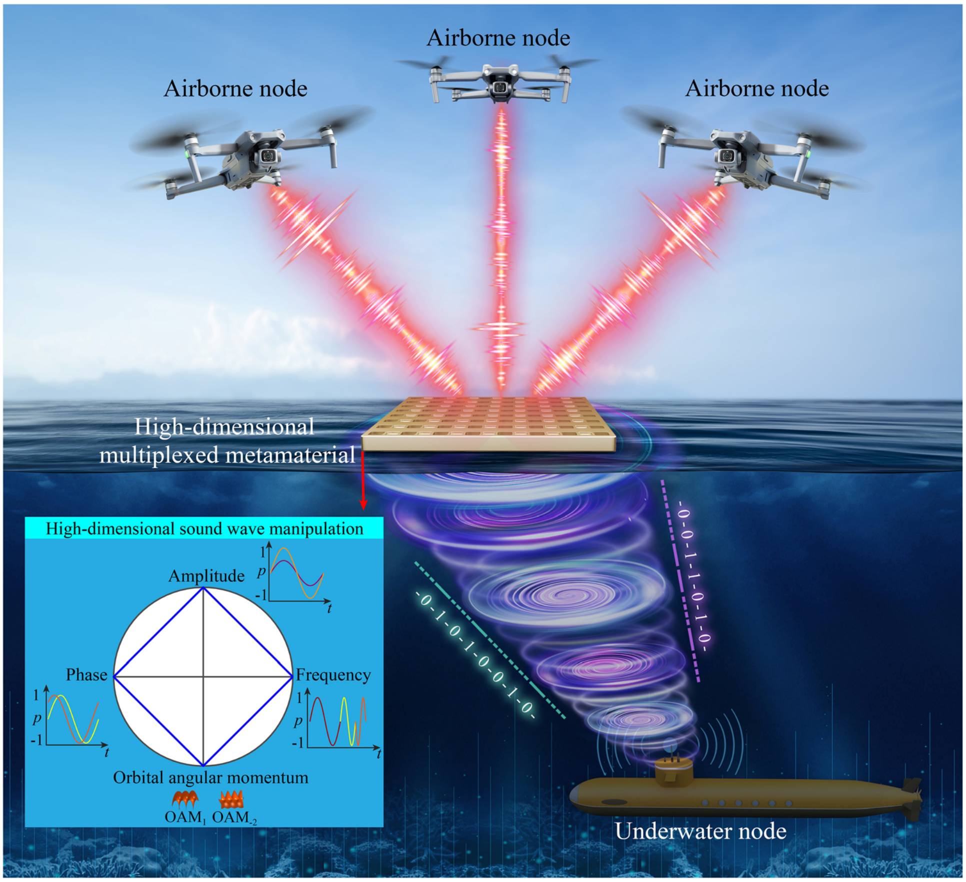

Fig. 1 Schematic of HDM metamaterial for high-speed all-sound communication across the water–air media. The underwater node emits multi-frequency and multi-OAM-mode synthesized sound beams, with each beam serving as an independent channel carrying different data streams. At the water–air interface, the HDM metamaterial with planar profile and subwavelength thickness receives the underwater synthesized OAM beams and relays them to multiple airborne spatially-separated beams in a high-efficiency, real-time and no-carrier-conversion paradigm. The inset illustrates the all-dimensional manipulation of the cross-media sound wave (amplitude, phase, frequency, and OAM) through the designed HDM metamaterial. Above the water, multiple airborne communication nodes receive in real-time the demultiplexed acoustic signals with low crosstalk.

challenging. For example, although OAM of different modes, serving as an infinite orthogonal basis in spatial dimension, has shown great potential in boosting channel capacity and transmission speed, OAM-based spatial multiplexing communication has only been achieved in homogeneous media, while its implementation across different media still remains unexplored. These challenges are primarily attributed to the lack of ability of existing materials for multi-dimensional sound wave control in inhomogeneous media. Here, we overcome the aforementioned limitations by proposing a passive and compact HDM metamaterial that significantly expands the controllable dimensions of cross-media sound waves. Based on this, an example of cross-media all-sound communication is demonstrated, wherein the HDM metamaterials operate as a passive meta-repeater that merges the functions of both relay and decoder within the subwavelength size, as will be discussed later.

As shown in Fig. 1, considering an underwater node emitting a synthesized acoustic beam consisting of several coaxially overlapping vortex beams with different OAM modes and frequencies, which serve as independent channels for encoding different data streams, the multiplexed acoustic pressure distribution on the transmitting array can thus be written as

$$p(\theta,t)=\sum_{n=1}^{N}A_n(t)\exp\{i[\omega_m t+l_n\theta+\varphi_n(t)]\}\quad (m=1,2,\cdots,M) \tag{1}$$

where M frequency components and N OAM modes are employed for spectral and spatial multiplexing, respectively, $\omega_m = 2\pi f_m$ is the angular frequency of each spectral component, and θ is the azimuthal angle. $A_n(t)$ and $\varphi_n(t)$ represent the time-dependent data streams encoded on the amplitude and phase of the l_nth-order OAM beam, respectively. Therefore, eqn (1) encompasses all dimensions of sound waves, including frequency, phase, amplitude, and OAM, and illustrates how information is encoded in these dimensions. At the water–air interface, the HDM metamaterial with planar profile and subwavelength thickness receives and relays the underwater information carried by the incident underwater synthesized vortex beams to several airborne spatially-separated receiving nodes. To this end, the HDM metamaterials must possess the ability to effectively modulate all relevant dimensions of cross-media sound waves, as determined by eqn (1). This means that in addition to matching the acoustic impedance of water and air at multiple frequencies, the HDM metamaterial also needs to be imposed with a frequency-dependent phase pattern for OAM decoding in physical space. To theoretically derive the expression of such a phase profile, we begin from the simplest case of a single OAM mode. For an incident vortex beam carrying the topological charge l_n at working frequency f_m, we encode the HDM metamaterials with an anti-spiral phase distribution $-l_n\theta$, so that only when an incident wave carries OAM of order l_n can its chirality be removed to yield a plane wave, whereas incidence with other OAM orders merely results in a change of the OAM order. Then, a radial phase term $\exp(-ik_m r_n)$ is imposed to focus and redirect the outgoing wavefront to a prescribed detection position $F_n = (x_n, y_n, z_n)$, where $k_m = \omega_m/c_0$ is the wavenumber, c_0 = 343 m s^{-1} is the sound speed in air, and $r_n = \sqrt{(x-x_n)^2+(y-y_n)^2+(z-z_n)^2}$ is the distance between the HDM metamaterial (x, y, z) and F_n. The multi-dimensional decoding can be realized by superposing multiple OAM- and frequency-dependent responses on the HDM metamaterial, as follows

$$\varphi = \arg\left\{\sum_{n,m}^{N} \exp[i(-l_n)\theta - ik_m r_n]\delta(f_0, f_m)\right\} \quad (2)$$

where f_0 is the frequency of the incident wave, and δ is the Kronecker delta function. Physically, eqn (2) contains two key terms, namely, an azimuthal phase-conjugation term for OAM-selective decoding and a focusing phase term for spatial separation of different modes. At the receiving end, our mechanism allows one to utilize only a single airborne sensor mounted on the pre-designed airborne communication node at F_n to receive the high-SNR (signal-to-noise ratio) demodulated signal while requiring neither sophisticated sensor array nor time-consuming postprocessing. It can therefore be expected that our proposed HDM metamaterial provides a new paradigm for extending high-dimensional acoustic communication and sound wave manipulation to complex cross-media systems.

2.2. The structural design of HDM metamaterial

For conventional single-layered anti-reflection materials, whether natural or artificial, the well-known quarter-wavelength condition dictates that at resonance frequencies where unity sound energy transmission occurs, the transmission phase is constrained to $\pm\pi/2$, resulting in the inherent amplitude-phase trade-off. To overcome this and implement our multi-dimensional modulation mechanism, here we propose a novel structural design of HDM metamaterial by introducing multilayered impedance design and spatially hybridized resonators, as shown in Fig. 2a. Specifically, the former (namely, multilayered impedance design) breaks through the limitations of traditional single-layered structural design in terms of resonance-induced phase and frequency-locking while the latter can significantly extend the number of working frequency components. As a result, the HDM metamaterial enables full-range amplitude and phase modulation across multiple working frequencies in inhomogeneous media and its assembly allows arbitrary wavefront reconstruction for OAM demodulation, as will be demonstrated in the following.

For simplicity while without losing generality, here we showcase a simple structural design with two subunits wherein each subunit corresponds to a different operation frequency: f_1 = 12 kHz and f_2 = 16 kHz. The layers a and c, shaped as square air cavities (marked in dark brown) at both ends of each subunit, are designed to modulate the amplitude of cross-media waves by adjusting the acoustic impedance matching conditions with air and water respectively, whose effective acoustic impedance is controlled by the widths of the air cavities. In our demonstrated full-DoFs control over sound waves, layers a and c are specifically designed as perfect resonance matching layers to enable near-unity transmission efficiency. Besides, their resonance feature also ensures that acoustic waves at the specific frequency interact exclusively with their corresponding subunit, without penetrating into the other, thereby providing strong frequency selectivity. The middle layer b (marked in light brown), featuring a length-varying air slit, introduces an adjustable phase delay to the transmitted wave by folding the propagation path, thereby allowing precise manipulation of the transmitted wavefront within subwavelength spatial resolution. The design details and geometrical parameters are given in the SI Note S1.

We first use numerical simulation to demonstrate the frequency modulation performance of the HDM metamaterial. Fig. 2b (left) shows the calculated transmission curves of two subunits within the frequency range of 10 kHz to 18 kHz, with L_1 = 33 mm and L_2 = 31.6 mm. It can be observed that the transmission coefficient of subunit 1 (0.61) is much higher than that of subunit 2 (0.057) at f_1 = 12 kHz, while subunit 2 exhibits a much higher transmission coefficient (0.59) than subunit 1 (0.018) at f_2 = 16 kHz. To quantitatively characterize the spectral selectivity and crosstalk of the HDM metamaterial, we introduce two parameters of −3 dB bandwidths and inter-channel isolation degree ($\mathrm{Iso}(f_k)$), respectively. From the numerically simulated transmission spectra in Fig. 2b, the −3 dB bandwidths can be calculated to be 1360 Hz for subunit 1 and 820 Hz for subunit 2 (fractional bandwidths of 11.3% and 5.1%, respectively). Another parameter of inter-channel isolation degree is defined as the logarithmic ratio of the energy transmission of subunit k at the operating spectral component f_k to the maximum transmission coefficient among all the other subunits,

$$\mathrm{Iso}(f_k) = 10\log_{10}\left(\frac{|t_k(f_k)|^2}{\max_{m\neq k}|t_m(f_k)|^2}\right). \quad (3)$$

A larger value of $\mathrm{Iso}(f_k)$ indicates more suppressed transmission leakage from subunits other than subunit k at f_k. Accordingly, the isolation degrees reach $\mathrm{Iso}(f_1) \approx 20.6$ dB and $\mathrm{Iso}(f_2) \approx 30.3$ dB, suggesting that the transmitted energy contributed by subunits not corresponding to the operating frequency is less than 1%. For a clear illustration, we simulate the acoustic

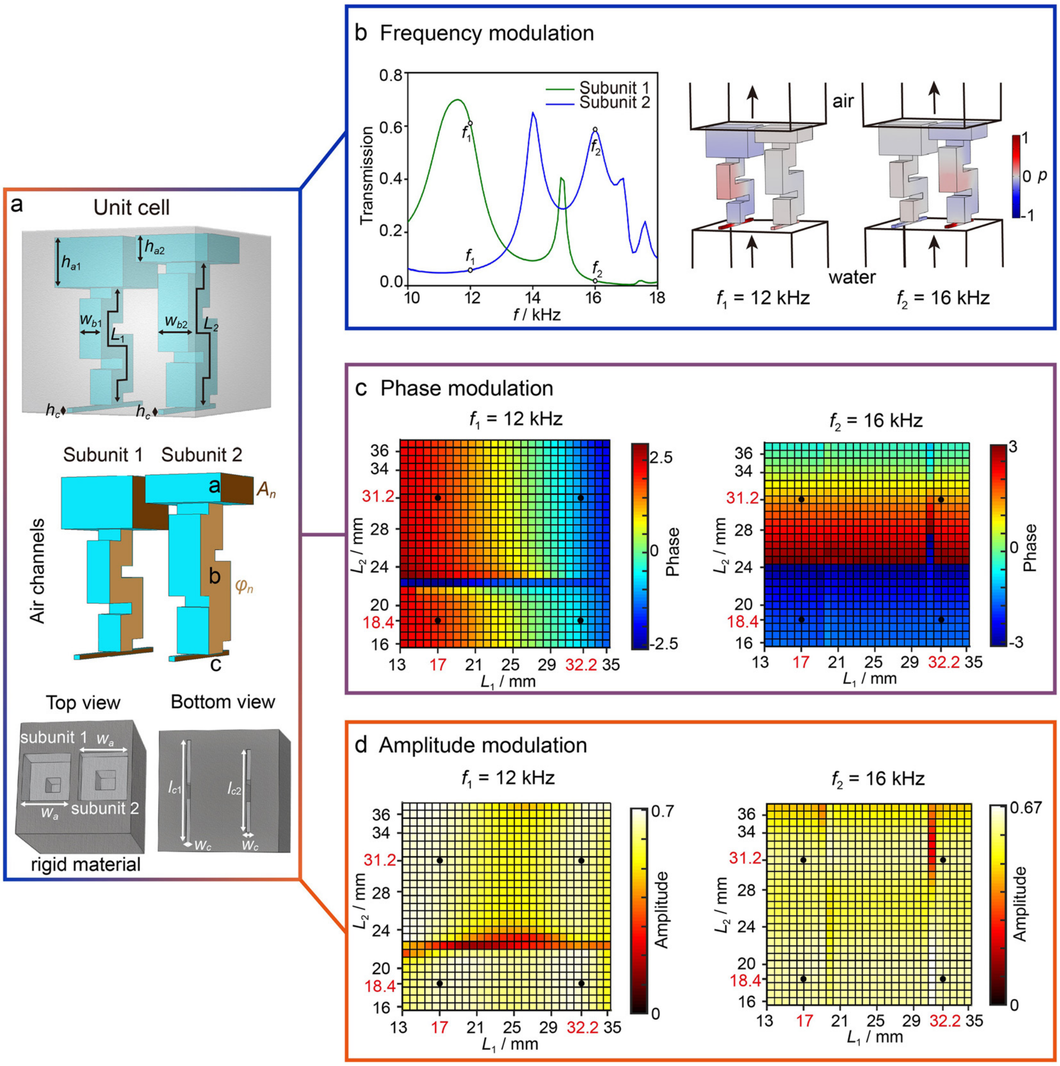

Fig. 2 The HDM metamaterial for modulating all dimensions of cross-media sound waves, including frequency, phase and amplitude. (a) The designed HDM metamaterial unit consisting of two subunits corresponding to different central frequencies, formed by slotting the cube rigid material with judiciously designed air channels. Each subunit is composed of three layers of a, b and c, where layers a and c serve as impedance matching layers contacting with air and water respectively and layer b introduces a tunable phase shift by changing its length. (b) Demonstration of frequency modulation. Left: The transmission curves of two subunits from 10 to 18 kHz with L_1 = 33 mm, L_2 = 31.6 mm. Right: The acoustic pressure fields in the whole hybrid structure at f_1 = 12 kHz and f_2 = 16 kHz, respectively. The arrows indicate the incident and transmission directions. (c) The phase and (d) amplitude responses of the designed HDM metamaterial unit as a function of the parameters L_1 and L_2 at f_1 and f_2 respectively.

pressure distribution through the whole HDM metamaterial composed of these subunits at f_1 and f_2, respectively. The results shown in Fig. 2b (right) indicate that the response of subunit 1 (2) is dominant when f_1 (f_2) is incident, while the response of subunit 2 (1) only produces negligible background noise. Next, we showcase the capabilities of our designed HDM metamaterial unit in precise amplitude and phase control at two discrete working frequencies. From the typical results with the viscothermal effect being taken into account in Fig. 2c and d, we can observe that within the investigated parameter space, a linear phase shift covering the full 2π range for each incident spectrum component can be achieved by tuning the single structural parameter L_i (i = 1, 2) while maintaining a significantly large sound transmission enhancement over 156 times compared to the bare water–air interface. This validates that in our design scheme, two subunits can be nearly decoupled from each other, enabling independent modulation on the incident signals of different frequencies, which is beyond attainable with the existing anti-reflection materials. Notice that the effective frequency channel number can be further boosted by increasing the density of resonance states in the cross-media coupling HDM metamaterial (see another HDM metamaterial unit design with more frequency channels in SI Note S2).

2.3. The HDM metamaterial-based meta-repeater for cross-media communication system

Then, we demonstrate an example of direct cross-media all-sound communication with the HDM metamaterial serving as a novel passive meta-repeater. For facilitating the proof-of-concept experiment, here we develop a particular meta-repeater constructed with 12 × 12 metamaterial units and choose to demonstrate a four-channel cross-media all-sound communication system by marrying frequency multiplexing with OAM multiplexing [*i.e.*, two frequency channels × two OAM channels (l_1 = +1 and l_2 = −1)]. The phase distributions on the monolayered meta-repeater, calculated by eqn (2), are depicted in Fig. 3a for the demultiplexing of two-mode vortex beams at two working frequencies. In our design, the detection points of 1st-order and -1st-order vortex beams are set as F_1 (0, 0.08 m, 0.2 m) and F_2 (0, −0.08 m, 0.2 m), respectively. For simplifying the meta-repeater design, binary phases of 0 and π are applied to replace the continuous phase values on the profile (see SI Note S3 for details).[47–50] Based on this, we assemble a frequency-OAM-multiplexed passive meta-repeater using four basic HDM metamaterial units (marked by four dots in Fig. 2c), as shown in the bottom of Fig. 3a. Units 1 to 4 marked by "00" to "11" impose (0, 0), (0, π), (π, 0) and (π, π) phase delay on the incident waves at 12 kHz and 16 kHz respectively, while keeping high transmission efficiency to ensure optimal communication performance.

Experiments to verify the performance of our designed meta-repeater are carried out in a cross-water–air anechoic environment. Fig. 3b depicts the photography of the experimental setup and the 3D-printed prototype of the meta-repeater. At the transmitting terminal, a two-mode OAM (l_1 = +1, l_2 = −1) multiplexing system is established by a Field Programmable Gate Array (FPGA)-driven phased array with 8 evenly arranged underwater transducers (see SI Note S4 for details), as shown in Fig. 3c. The binary data streams of 0 and 1 are encoded into the generated vortex beam by modulating its amplitude, with each stream assigned to distinct channels in the amplitude dimension. After interacting with the meta-repeater positioned at the water–air interface, the two-mode two-frequency vortex beams carrying information are relayed and demodulated into two designated airborne nodes, each equipped with a microphone to capture the respective decoded signals in real-time, with no need of time-consuming sensor scanning and complicated post-processing algorithms. Additionally, our proposed HDM metamaterial-based cross-media communication mechanism, which uses sound waves with macroscopic wavelengths as the sole carrier, naturally resists electromagnetic interference and adverse weather conditions, making it inherently advantageous for practical applications.

2.4. Experimental realization of real-time and high-speed cross-media all-sound communication

In experiment, we first verified the performance of our HDM metamaterial-based meta-repeater for efficient OAM modulation. Fig. 4a and b presents 3D plots of the simulated and measured spatial distributions of acoustic intensity within two

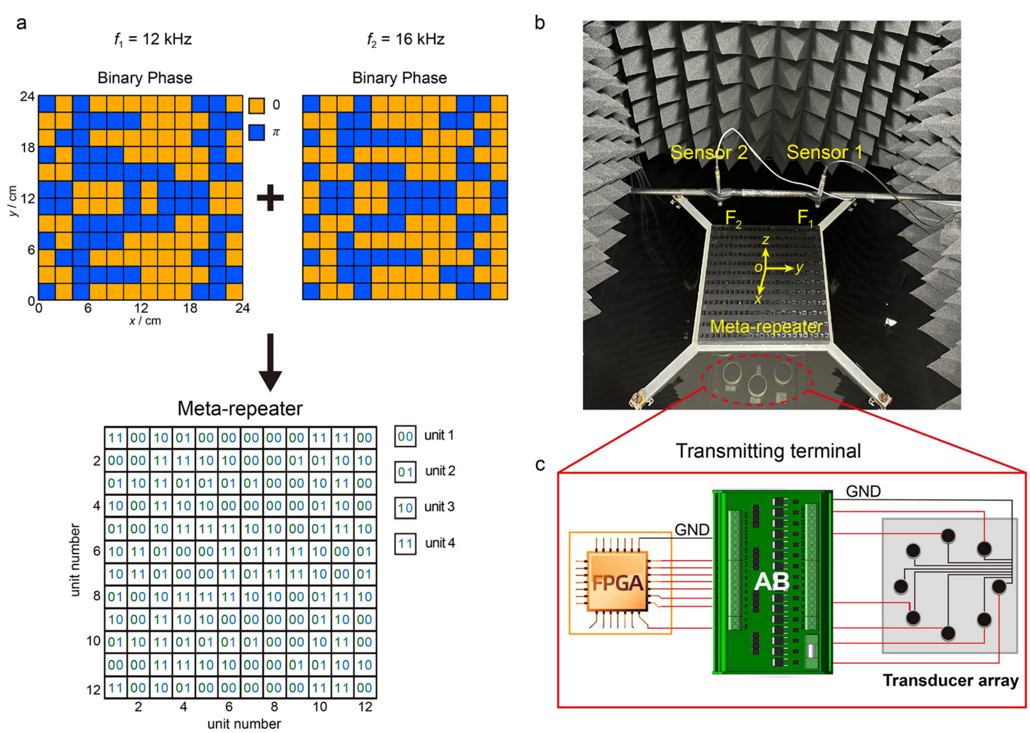

Fig. 3 The HDM metamaterial-based meta-repeater for spatial and spectral multiplexing and the experimental setup of cross-media all-sound communication system. (a) The binary phase distributions required for demodulating the synthesized OAM beams with topological charges l_1 = +1 and l_2 = −1 at f_1 and f_2 respectively, and the resulting spatially and spectrally-multiplexed meta-repeater constructed by a 12 × 12 array consisting of HDM metamaterial units. (b) Photograph of the experimental setup of cross-media all-sound communication system. The 3D-printed sample is placed on the water–air interface and two sensors are placed at two predesigned detection points marked by F_1 and F_2 to receive the demodulated signals. (c) The schematic diagram of the transmitting end of the communication system.

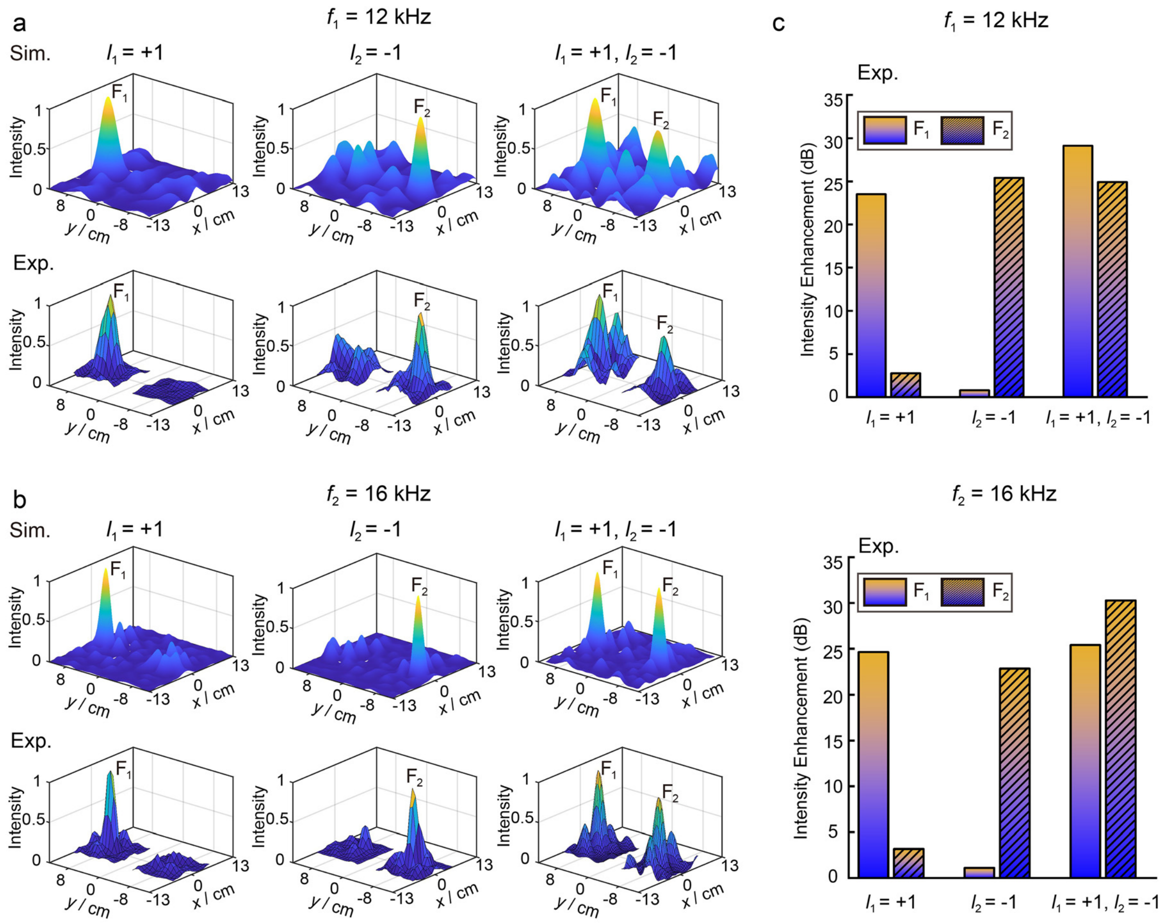

Fig. 4 The demonstration of the designed meta-repeater for high-efficiency sound energy transfer and OAMs demultiplexing through numerical simulations and experimental measurements. (a and b) The comparison between the measured and simulated sound intensity distributions within two square areas centered at two detection points respectively when different OAM channels are opened at (a) f_1 = 12 kHz and (b) f_2 = 16 kHz. (c) The histogram of measured intensity enhancements by the designed HDM metamaterial under different coding situations.

11.2 × 11.2 cm^2 square regions centered at F_1 and F_2 when different OAM channels are "turned on" at two operating frequencies, *e.g.*, in the leftmost figure, we only transmit an acoustic signal encoded into a 12 kHz vortex beam of l_1 = +1. For clearer comparison, we also measure the sound intensity distributions in a square area centered at F_1 without applying the meta-repeater at the water–air interface, for which the working OAM channel is 1st-order vortex beam at f_1 and f_2 respectively, as shown in Fig. S6. Good agreement between measured and simulated results can be observed in Fig. 4a and b, which show effective spatial separation of the multiplexed vortex beams with the expected energy convergence near their respective target detection points at two working frequencies, in contrast to the dark spot in the case of the bare water–air interface in Fig. S6 (see SI Note S5). The high energy contrast between the focal points of working and non-working OAM channels provides the innate robustness of our mechanism against channel crosstalk, which is vital for improving data decoding accuracy. Then we quantitatively evaluate the signal intensity enhancement brought by the designed HDM metamaterial by experimentally measuring the sound intensity at two detection points for all coding situations, both with and without the meta-repeater on the water–air interface, and calculate the resulting intensity enhancement values, as shown in Fig. 4c. The results reveal a large improvement in receiving sensitivity exceeding 23 dB at the target location when the corresponding channel is opened, confirming the HDM metamaterial's ability to modulate the amplitude of cross-media sound waves for optimal transmission. Consequently, we have comprehensively demonstrated the effective manipulation on all dimensions of cross-media sound waves by HDM metamaterial and its assembly, including amplitude, phase, frequency, and OAM.

Next, we demonstrate the effectiveness of the meta-repeater for direct cross-media all-sound communication *via* a practical example of real-time and high-speed transmission of a complicated four-bit grayscale image including 338 × 460 pixels shown in Fig. 5a. Fig. 5b (left) shows an enlarged view of a particular column of pixels marked by the red line in Fig. 5a, wherein the gray level of each pixel corresponds to a 4-bit data. In our implementation, two-mode dual-frequency vortex beams are utilized as four independent channels, marked as Ch*i* (i = 1,

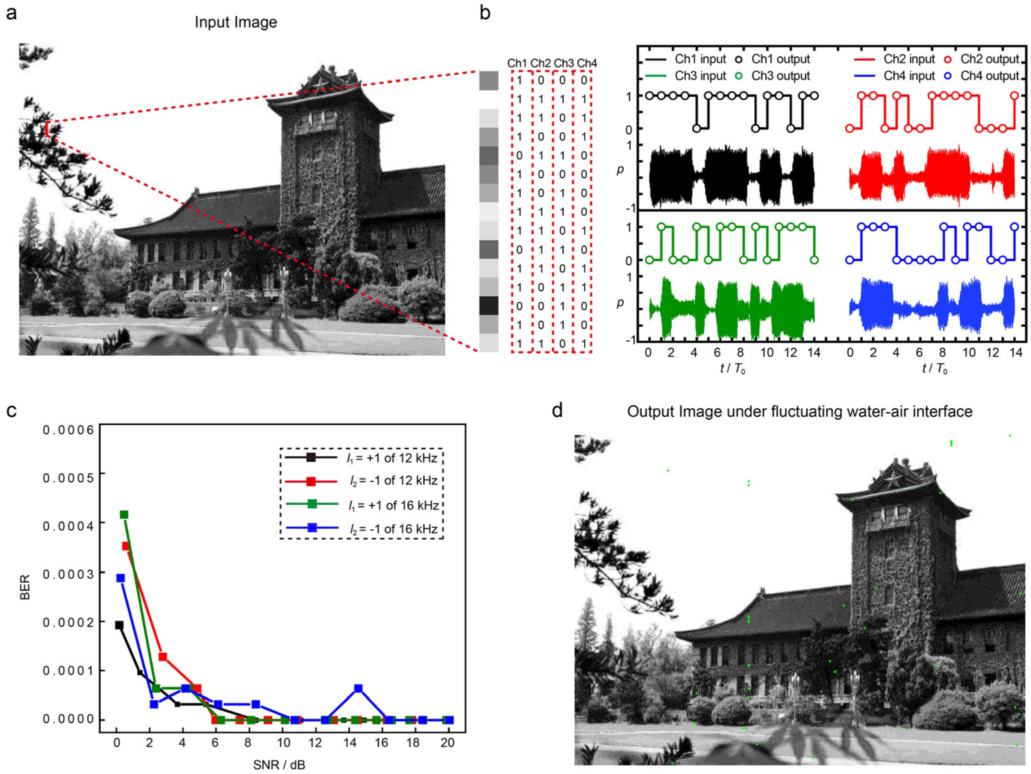

Fig. 5 Experimental results of real-time cross-media all-sound communication of a four-bit grayscale image. (a) The original input image which is transmitted by four independent channels (*viz.*, Ch1, Ch2, Ch3 and Ch4 respectively). (b) Left: The enlarged view of a particular column of pixels marked by the red line in (a) and the *i*-th data of each pixel is transmitted by Ch*i*. Right: The comparison between the input and output results of four data streams corresponding to the pixels on the left, and the measured time-domain signals in each pulse period in four channels. (c) The measured BERs of four channels *versus* SNR. (d) The output image of the communication system under fluctuating water–air interface, and the green dots represent the wrong pixels.

2, 3, 4), to transmit *i*-th data of each pixel in 2ASK (binary amplitude shift keying) format. The data-carrying signal is in pulse modulation with a pulse period of T_0 = 1.6 ms and each pulse cycle contains 1-bit data such that the communication speed of our cross-media system can reach 2500 bit per s. At the operating frequencies of 12 kHz and 16 kHz, T_0 contains about twenty acoustic cycles, so that each "0/1" bit is represented by a sufficiently long quasi-steady sinusoid segment, keeping the dominant spectral components concentrated near the designated discrete frequency lines and suppressing spectral leakage. In addition, this pulse period enables inserting "0" symbols as guard intervals between data segments to mitigate the influence of the residual ringing and multipath reflections, thereby reducing inter-symbol interference without excessively compromising the communication rate. Fig. 5b shows the comparison between the four time-domain signals received by airborne sensors and the four input data streams corresponding to the pixels on the left. For extracting data streams from the time-domain signals, we perform the cross-correlation between the received signals and an ideal sinusoidal signal of working frequency and plot the decoded data streams in Fig. 5b (marked by dots), which are fully consistent with the input ones. By assembling four decoded data streams of four channels together, we obtain a high-quality output image without any bit errors, validating the effectiveness of the proposed mechanism. Notice that the communication speed can be further improved by increasing the number of OAM channels and applying high-order modulation technology to encode data or shortening the pulse modulation period (see SI Note S6 for another example with higher communication speed).

We also quantitatively evaluate the accuracy of data transfer in our demonstrated cross-media communication system at different SNR levels. By increasing the ambient noises in the air, we vary the SNR of the received signal and then experimentally measure the BERs of the recovered four-bit grayscale image as a function of SNR (see Fig. 5c). Here, the BER is defined as the ratio of the number of error decoding data to the total number of transmitted data. It can be observed that the BERs of all four channels are close to 0 at a SNR level of more than 8 dB and increase with the decrease of SNR, as expected. Meanwhile, the BER of the whole communication system remains about one order of magnitude lower than the FEC limit of 3.8×10^{-3} even at an extremely low SNR level, which manifests the system's high accuracy and strong resistance to noise interference. To further investigate the applicability of our meta-repeater in a real-world system, we agitate the water surface to simulate an actual fluctuating environment and measure the BER of the transmitted image in this case.

Specifically, the interface fluctuation was produced by manually oscillating a glass plate ($\approx$5 cm $\times$ 15 cm $\times$ 0.5 cm) at one corner of the tank, generating random and irregular surface water waves in the measurement region (see SI Video S1). The typical peak-to-peak surface displacement is on the order of 10–15 mm, corresponding to a root-mean-square amplitude of $\sigma \approx$ 4–6 mm, and the fluctuation period is approximately 0.5–1.0 s (*i.e.*, $\sim$1–2 Hz). At our operating frequencies (12 kHz and 16 kHz), the acoustic wavelength in water is $\lambda \approx$ 9/12.5 cm, giving a normalized interface roughness $\sigma/\lambda \approx 0.03/0.07$ (<0.1), indicating a weak-roughness regime that may induce certain perturbations in both phase and amplitude but not completely destroy the wavefront. The output image through the fluctuating water–air interface is plotted in Fig. 5d where the wrong pixels are marked by green dots and the measured BER is 2.5×10^{-4}, proving that the HDM metamaterial-based cross-media all-sound communication method can also work for the fluctuating water surface. More detailed robustness analyses for stronger surface roughness ($\sigma/\lambda > 0.1$) as well as volume turbulence and multipath effects in realistic sea environments are provided in SI Note S7. Although here we only demonstrate a simple case with a relatively short communication distance due to the limited experiment space, our mechanism can apply to remote cross-media all-sound communication by optimally designing the transmitting array and HDM metamaterial-based meta-repeater (see SI Note S8 for the demonstration of a km-scale cross-media all-sound communication system). To more clearly demonstrate the superiority of the developed HDM metamaterial and single-carrier acoustic communication mechanism, we also provide qualitative and quantitative comparisons between our method and several representative prior works in SI Tables S3 and S4.

3. Conclusion

To conclude, we have proposed and experimentally demonstrated a HDM metamaterial capable of modulating cross-media sound waves across multiple dimensions, including amplitude, phase, frequency and OAM, based on which a meta-repeater is constructed to achieve real-time and high-speed cross-media all-sound communication. Our proposed monolayered HDM metamaterial-based meta-repeater working as an acoustic bridge to connect water and air, not only relays the underwater sound to airborne acoustic wave free of carrier conversion, but also enables flexible demodulation on the high-capacity complicated acoustic signals multiplexed by OAM and frequency. The effectiveness of the HDM metamaterial-based cross-media all-sound communication mechanism is demonstrated both numerically and experimentally *via* real-time and high-speed transmission of a complicated four-bit grayscale image across water–air media, showing a BER much lower than 1/10 of the FEC limit and high robustness to water surface fluctuation and background noise. Despite the relatively low number of OAM modes and short communication distance we demonstrate currently given the limitations of experimental conditions, it is obvious that our scheme is general and has no constraints on these performance parameters. We anticipate that our HDM metamaterial, with its ability to fully modulate all relevant dimensions of sound waves, will expand applications across a wide range of cross-media acoustic scenarios, such as transcranial ultrasound imaging and cross-media particle manipulation.

4. Experimental section

4.1. Numerical simulations

Throughout the paper, the simulations are conducted with a finite element method based on COMSOL MULTIPHYSICS software. The mass density and sound speed of air are set as ρ_a = 1.21 kg m^{-3} and c_a = 343 m s^{-1}, respectively. The mass density and sound speed of water are set as ρ_w = 1000 kg m^{-3} and c_w = 1490 m s^{-1}, respectively. The solid material for building the designed HDM metamaterial is chosen as UV resin whose mass density and sound speed are 1400 kg m^{-3} and 2000 m s^{-1}, respectively.

4.2. Experimental measurements

In the underwater part, a water tank with sound-absorbing rubber mounted on the boundary was built to mimic an anechoic environment. A transducer array with eight underwater transducers driven by FPGA was placed at the bottom center. The sample of HDM metamaterial-based meta-repeater is fabricated *via* 3D printing technology. The transmitted airborne sound signal at each focal point was measured in a 3D air anechoic chamber using a 1/4-in. Free-field microphone (Brüel & Kæjr type-4961). The real-time signals were recorded with Brüel & Kæjr PULSE 3160-A-042 4-channel analyzer.

4.3. Signal processing and decoding

In the experiments, we use 2ASK to encode the data, where the transmitted bit 0/1 is encoded into the amplitude of the carrier within each symbol interval. The received time-domain signals directly reflect the amplitude information of the corresponding channel, which is extracted through the cross-correlation method. Concretely, for each symbol interval, we compute the normalized cross-correlation between the received waveform and an ideal reference sinusoid at the assigned carrier frequency, with the reference length equal to one pulse period. The resulting peak correlation value is used as the decision statistic. A fixed threshold (0.5 in our implementation) is set as the decision criterion: values exceeding the threshold are decoded as a transmitted bit "1", while those below the threshold are decoded as "0". This correlation operation acts as a matched filtering process, enabling selective extraction of the component at the target carrier frequency while strongly suppressing broadband noise. In this manner, different OAM-frequency channels are decoded in parallel by applying the same processing chain to the recordings from the microphones located at the corresponding focal point, followed by correlation with the channel-specific reference frequency.

Author contributions

Kai Wu: conceptualization, methodology, software, validation, visualization and writing– original draft. Jing-Jing Liu: conceptualization, methodology, software, validation and writing – original draft. Hao-Xiang Li: validation. Xue-Feng Zhu: writing – original draft. Bin Liang: conceptualization, investigation, supervision, funding acquisition and writing– original draft. Jian-Chun Cheng: funding acquisition, supervision and writing – original draft. Johan Christensen: supervision and writing – original draft.

Conflicts of interest

The authors have no conflicts to disclose.

Data availability

The data supporting this article have been included as part of the supplementary information (SI). Ref. 51–54 are cited in the SI. Supplementary information: supplementary note 1, the design of acoustic frequency-multiplexed water–air coupling HDM metamaterial, supplementary note 2, the increase in the number of frequency channels, supplementary note 3, the analysis of the influence of phase discretization on the OAMs demultiplexing, supplementary note 4, encoding information into the multiplexed acoustic vortex beams using an active underwater transducer array, supplementary note 5, the measured sound distributions on the output plane without the HDM metamaterial at the water–air interface, supplementary note 6, the realization of higher transmission speed of our proposed cross-water–air all-sound communication system, supplementary note 7, robustness analysis under realistic sea-surface conditions, and supplementary note 8, the realization of km-scale all-sound communication across the water–air interface. See DOI: https://doi.org/10.1039/d5mh02182k.

Acknowledgements

This work was supported by the National Key R&D Program of China (Grant No. 2022YFA1404402), the National Natural Science Foundation of China (Grant No. 12304493 and 12174190), Natural Science Foundation of Jiangsu Province (Grant No. BK 20230767), the Fundamental Research Funds for the Central Universities (Grant No. KG202501), High-Performance Computing Center of Collaborative Innovation Center of Advanced Microstructures and a project funded by the Priority Academic Program Development of Jiangsu Higher Education Institutions. J. J. L. acknowledges the support from Young Elite Scientists Sponsorship Program by CAST (Grant No. 2023QNRC001).

Notes and references

1 M. Horodynski, M. Kühmayer, C. Ferise, S. Rotter and M. Davy, *Nature*, 2022, **607**, 281–286.
2 O. A. Godin, *Contemp. Phys.*, 2008, **49**, 105–123.
3 Z.-H. Peng and L.-S. Zhang, *Chin. Phys. B*, 2016, **25**, 124306.
4 E. Dong, Z. Song, Y. Zhang, S. Ghaffari Mosanenzadeh, Q. He, X. Zhao and N. X. Fang, *Sci. Adv.*, 2020, **6**, eabb3641.
5 A. Wang, L. Zhu, Y. Zhao, S. Li, W. Lv, J. Xu and J. Wang, *Opt. Express*, 2018, **26**, 8669–8678.
6 A. P. Voloshchenko and S. P. Tarasov, *J. Acoust. Soc. Am.*, 2019, **145**, 143–148.
7 J. Li, W. Li, Q. Liu, B. Luo and W. Cui, *Ocean-Land-Atmos. Res.*, 2024, **3**, 0036.
8 Z. Ren, H.-W. Dong, S.-D. Zhao, M. Chen and D. Fang, *Phys. Rev. Appl.*, 2024, **22**, 024023.
9 P. C. Pedersen, O. Tretiak and P. He, *J. Acoust. Soc. Am.*, 1982, **72**, 327–336.
10 B. Assouar, B. Liang, Y. Wu, Y. Li, J.-C. Cheng and Y. Jing, *Nat. Rev. Mater.*, 2018, **3**, 460–472.
11 S. A. Cummer, J. Christensen and A. Alù, *Nat. Rev. Mater.*, 2016, **1**, 16001.
12 J.-J. Liu, Y.-J. Ding, K. Wu, B. Liang and J.-C. Cheng, *Appl. Phys. Lett.*, 2021, **119**, 213502.
13 G. Ma and P. Sheng, *Sci. Adv.*, 2016, **2**, e1501595.
14 H. X. Li, M. Rosendo-López, Y. F. Zhu, X. D. Fan, D. Torrent, B. Liang, J. C. Cheng and J. Christensen, *Research*, 2019, **2019**, 8345683.
15 Q. Song, X. Liu, C.-W. Qiu and P. Genevet, *Appl. Phys. Rev.*, 2022, **9**, 011311.
16 J. Zhang, N. Zhou, E. Dong, C. Zhang, Z. Song, S. Liu, C. Yang, X. Su, S. Wang and Y. Zhang, *Matter*, 2024, **7**, 3857–3875.
17 C. Della Giovampaola and N. Engheta, *Nat. Mater.*, 2014, **13**, 1115–1121.
18 T. J. Cui, M. Q. Qi, X. Wan, J. Zhao and Q. Cheng, *Light: Sci. Appl.*, 2014, **3**, e218.
19 O. A. Godin, *Phys. Rev. Lett.*, 2006, **97**, 164301.
20 A. Bretagne, A. Tourin and V. Leroy, *Appl. Phys. Lett.*, 2011, **99**, 221906.
21 E. Bok, J. J. Park, H. Choi, C. K. Han, O. B. Wright and S. H. Lee, *Phys. Rev. Lett.*, 2018, **120**, 044302.
22 Z. Cai, S. Zhao, Z. Huang, Z. Li, M. Su, Z. Zhang, Z. Zhao, X. Hu, Y. S. Wang and Y. Song, *Adv. Funct. Mater.*, 2019, **29**, 1906984.
23 T. Lee and H. Iizuka, *Phys. Rev. B*, 2020, **102**, 104105.
24 Z. Huang, S. Zhao, Y. Zhang, Z. Cai, Z. Li, J. Xiao, M. Su, Q. Guo, C. Zhang and Y. Pan, *Research*, 2021, **2021**, 9757943.
25 Z. Huang, Z. Zhao, S. Zhao, X. Cai, Y. Zhang, Z. Cai, H. Li, Z. Li, M. Su and C. Zhang, *ACS Appl. Mater. Interfaces*, 2021, **13**, 53242–53251.
26 X.-T. Gong, H.-T. Zhou, S.-C. Zhang, Y.-F. Wang and Y.-S. Wang, *Appl. Phys. Lett.*, 2023, **123**, 231703.
27 J. Liu, Z. Li, B. Liang, J.-C. Cheng and A. Alù, *Adv. Mater.*, 2023, **35**, 2301799.
28 H. T. Zhou, S. C. Zhang, T. Zhu, Y. Z. Tian, Y. F. Wang and Y. S. Wang, *Adv. Sci.*, 2023, **10**, 2207181.
29 Y.-Z. Tian, R. Li, Y.-F. Wang, V. Laude and Y.-S. Wang, *Phys. Rev. B*, 2024, **110**, 214101.
30 S.-C. Zhang, H.-T. Zhou, X.-T. Gong, Y.-F. Wang and Y.-S. Wang, *J. Sound Vib.*, 2024, **575**, 118269.
31 L. Shi, T. Zhu, Y.-L. Du, H.-T. Zhou, Y.-Z. Tian, Y.-F. Wang and Y.-S. Wang, *Eng. Struct.*, 2025, **341**, 120611.

32 H. T. Zhou, C. Y. Li, J. H. Zhu, C. Hu, Y. F. Wang, Y. S. Wang and C. W. Qiu, *Adv. Mater.*, 2024, **36**, 2313004.
33 Y. Yan, G. Xie, M. P. Lavery, H. Huang, N. Ahmed, C. Bao, Y. Ren, Y. Cao, L. Li and Z. Zhao, *Nat. Commun.*, 2014, **5**, 4876.
34 A. E. Willner, H. Huang, Y. Yan, Y. Ren, N. Ahmed, G. Xie, C. Bao, L. Li, Y. Cao and Z. Zhao, *Adv. Opt. Photonics*, 2015, **7**, 66–106.
35 X. Jiang, Y. Li, B. Liang, J.-C. Cheng and L. Zhang, *Phys. Rev. Lett.*, 2016, **117**, 034301.
36 C. Shi, M. Dubois, Y. Wang and X. Zhang, *Proc. Natl. Acad. Sci. U. S. A.*, 2017, **114**, 7250–7253.
37 X. Jiang, B. Liang, J. C. Cheng and C. W. Qiu, *Adv. Mater.*, 2018, **30**, 1800257.
38 J.-j Liu, B. Liang and J.-c Cheng, *Phys. Rev. Appl.*, 2021, **15**, 014015.
39 M. Solyanik-Gorgone, J. Ye, M. Miscuglio, A. Afanasev, A. E. Willner and V. J. Sorger, *Research*, 2021, **2021**, 9757943.
40 K. Wu, J.-J. Liu, Y.-J. Ding, W. Wang, B. Liang and J.-C. Cheng, *Nat. Commun.*, 2022, **13**, 5171.
41 A. E. Willner, K. Pang, H. Song, K. Zou and H. Zhou, *Appl. Phys. Rev*, 2021, **8**, 041312.
42 A. Jamshidi, *Wirel. Netw.*, 2019, **25**, 4815–4827.
43 H. Luo, X. Xie, G. Han, R. Ruby, F. Hong and Y. Liang, *IEEE Access*, 2019, **7**, 134954–134967.
44 Z. Ji, Y. Fu, J. Li, Z. Zhao and W. Mai, *IEEE Commun. Mag.*, 2021, **59**, 140–143.
45 H. Luo, J. Wang, F. Bu, R. Ruby, K. Wu and Z. Guo, *IEEE Sens. J.*, 2022, **22**, 8360–8382.
46 T. Richter, E. Palushani, C. Schmidt-Langhorst, R. Ludwig, L. Molle, M. Nolle and C. Schubert, *J. Lightwave Technol.*, 2011, **30**, 504–511.
47 H. Zhang, Q. Wang, M. Fink and G. Ma, *Nat. Commun.*, 2024, **15**, 1270.
48 G. Ma, X. Fan, P. Sheng and M. Fink, *Proc. Natl. Acad. Sci. U. S. A.*, 2018, **115**, 6638–6643.
49 Q. Wang, P. del Hougne and G. Ma, *Phys. Rev. Appl.*, 2022, **17**, 044007.
50 Q. Wang, M. Fink and G. Ma, *Phys. Rev. Appl.*, 2023, **19**, 034084.
51 E. I. Thorsos, *J. Acoust. Soc. Am.*, 1988, **83**, 78–92.
52 S. Pan, L. Wang, W. Wang and S. Zhao, *Sci. Rep.*, 2019, **9**, 14009.
53 H. Chang, X. Yin, X. Cui, X.-Z. Chen, Y.-Z. Su, J.-X. Ma, Y.-J. Wang, L. Zhang and X. Xin, *Appl. Opt.*, 2019, **58**, 6085–6090.
54 S. Li and J. Wang, *Sci. Rep.*, 2017, **7**, 43233.

